Chemistry
A European
Journal

Chemistry Europe
European Chemical Societies Publishing

Accepted Article

Title: Revisiting the mechanism of asymmetric Ni-catalyzed reductive carbo-carboxylation with CO2: The additives affect the product selectivity

Authors: Ljiljana Pavlovic, Bjørn Carvalho, and Kathrin Helen Hopmann

To be cited as: *Chem. Eur. J.* **2024**, e202401631

Link to VoR: https://doi.org/10.1002/chem.202401631

WILEY VCH

10.1002/chem.202401631

WILEY VCH

RESEARCH ARTICLE

Revisiting the mechanism of asymmetric Ni-catalyzed reductive carbo-carboxylation with CO_2: The additives affect the product selectivity

Ljiljana Pavlovic,*,[a] Bjørn Carvalho[a,b] and Kathrin H. Hopmann*,[a]

[a] Ljiljana Pavlovic, Bjørn Carvalho, Kathrin H. Hopmann
Department of Chemistry, UiT The Arctic University of Norway, N-9017 Tromsø, Norway.
E-mail: ljiljana.pavlovic@uit.no, kathrin.hopmann@uit.no

[b] Bjørn Carvalho
Hylleraas Center for Quantum Molecular Sciences, UiT The Arctic University of Norway, N-9017 Tromsø, Norway.

Supporting information for this article is given via a link at the end of the document.

Abstract: The mechanistic details of the asymmetric Ni-catalyzed reductive cyclization/carboxylation of alkenes with CO_2 have been revisited using DFT methods. Emphasis was put on the enantioselectivity and the mechanistic role of Lewis acid additives and *in situ* formed salts. Our results show that oxidative addition of the substrate is rate-limiting, with the formed Ni(II)-aryl intermediate preferring a triplet spin state. After reduction to Ni(I), enantioselective cyclization of the substrate occurs, followed by inner sphere carboxylation. Our proposed mechanism reproduces the experimentally observed enantiomeric excess and identifies critical C-H/O and C-H/N interactions that affect the selectivity. Further, our results highlight the beneficial effect of Lewis acids on CO_2 insertion and suggest that *in situ* formed salts influence if the 5-*exo* or 6-*endo* product will be formed.

Introduction

Carboxylic acids and their derivatives are versatile chemicals with widespread utilization in pharmaceutical, food and plastic industries.[1] Especially chiral carboxylic acids are of great interest in drug design, as biologically active molecules can be built from these compounds.[2]

During the past decades, metal-catalyzed carboxylation reactions with CO_2 have been employed to convert distinct substrates into their corresponding carboxylic acids.[3] In 2008, Rovis and co-workers reported one of the first examples of a catalytic Ni-mediated carboxylation of styrenes which could be performed under mild reaction conditions.[3a] Later, Martin`s group developed a Pd-catalyzed carboxylation of aryl bromides with CO_2 using $ZnEt_2$ as reducing agent.[3b] The same group disclosed the Ni-catalyzed carboxylation of benzylic halides with CO_2, Zn dust and $MgCl_2$.[3d] The use of the latter was found to be beneficial, as in the absence of $MgCl_2$, yields dropped. The authors speculated that Lewis acids (LAs) can facilitate CO_2 insertion into metal-alkyl bonds.[3d] Tsuji and co-workers reported the Ni-catalyzed carboxylation of aryl chlorides in the presence of Zn dust and ammonium-salt additives, whereas Douglas and co-workers developed a Cu-catalyzed carboxylation of aryl iodides with $ZnEt_2$ as reducing agent.[3i,3k] More challenging substrates included unactivated alkyl bromides possessing β-hydrogens, alkyl chlorides and bromocyclopropane derivatives.[3e-g,4]

The mechanistic details of metal-catalyzed carboxylations of organic (pseudo)halides with CO_2 have been studied intensively.[3k,3m,3o,5] On the basis of previous experimental[3k,3p,5a] and computational studies,[3p,5b-d] a general mechanism sets out from the oxidative addition of the substrate to a M^n complex, generating a M^{n+2}-alkyl species (**Scheme 1**). This is followed by Zn-[3d,3p,6] or Mn-mediated[3g,3k,4,7] reduction to give a reduced metal-alkyl[8] species, which can insert CO_2, either via an inner[8-9] or outer[9b,10] sphere pathway. The effect of Lewis acids such as $MgCl_2$ and LiCl on metal-alkyl carboxylations has been explored computationally, and it has been proposed that LAs accelerate CO_2 insertion by reducing the barrier for this step by several kcal/mol.[5b-d,11]

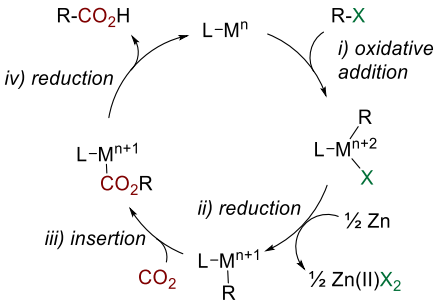

Scheme 1. General mechanism for the metal-catalyzed reductive carboxylation of organic (pseudo)halides with CO_2

In addition to developing protocols for carboxylation of aryls and styrenes, great efforts are also made towards the synthesis of (hetero)cyclic compounds bearing carboxylic acids. Formation of the latter can be promoted by metal-catalysts and CO_2 via so-called cascade reductive cyclization/carboxylation

10.1002/chem.202401631

reactions.[3f,3g,3m,3o,3p,6] One notable example is the intramolecular Ni-catalyzed cascade reductive cyclization/carboxylation of unactivated alkyl bromides using CO_2 and Mn as stoichiometric reductant to yield cyclo-fused acrylic acids.[3f] In 2021, Bandini and co-workers reported the first example of an asymmetric intramolecular Ni-catalyzed Heck-carboxylation with CO_2 and Zn to obtain 2,3-dihydrobenzofuran-3-ylacetic acids.[3p] Mechanistic DFT analysis indicated that after enantioselective cyclization, CO_2 inserts into an Ni(I)-alkyl complex. Computationally, also *ipso*-carboxylation was feasible with the Ni(I)-species, which contradicted experiments.[3p] Kong and co-workers have studied the Ni-catalyzed ligand-controlled regiodivergent reductive dicarbofunctionalization of alkenes.[12] Herein, the ligand determines the regioselectivity by favoring either 5-*exo* or 6-*endo* cyclization. This reaction proceeds under mild reaction conditions, with addition of $MgCl_2$ significantly increasing the yield.[12] Later, Yang`s group investigated the mechanistic details of this reaction, identifying factors that help explain how the ligand tunes the regioselectivity, but the effect of $MgCl_2$ was not studied.[13]

In 2021, Yu, Kong and co-workers developed an asymmetric Ni-catalyzed reductive carbo-carboxylation of methacrylamides with CO_2 (**Scheme 2**).[6] Diverse oxindole-3-acetic acid derivatives, which are important intermediates in the synthesis of bioactive natural products,[14] were synthesized under mild reaction conditions and with high chemo-, regio- and enantioselectivities.[6] Optimal reaction conditions were found in the presence of a $Ni(COD)_2$ pre-catalyst, Zn and the (S,S_p)-^{i}Pr-FOXAP ligand. Interestingly, side reactions such as *ipso*- and *endo*-carboxylations could be suppressed, and high yields of up to 98 % and enantiomeric excesses (*e.e.'s*) of up to 99.8 % (*R*) could be achieved. Addition of LiOtBu and $MgCl_2$ additives were essential for obtaining high yields.[6]

Based on the experimental work, two possible pathways for the Ni-mediated carboxylation of methacrylamides to the 5-*exo* product were proposed (**Scheme 3**).[6] In pathway **A**, oxidative addition of the R-X bond of the substrate to Ni(0) (**I**) forms a Ni(II)-(R)(X) intermediate (**II**), which undergoes single electron reduction to afford a Ni(I)-alkyl species (**III**). An enantioselective 5-*exo* cyclization produces intermediate **IV,** followed by CO_2 insertion to yield the Ni-carboxylate **VI**. Zn-mediated reduction regenerates species **I** and forms a Zn-carboxylate **VII**. Finally, acidic workup releases the carboxylated, 5-*exo*-product (**VIII**). The alternative mechanism **B** initially follows the same steps, however, the cyclization of the substrate occurs prior to reduction of Ni(II) to Ni(I) and dissociation of the halide. Thus, the two mechanistic proposals differ with respect to which reaction intermediate is mediating the enantioselective cyclization step. In addition, it is noteworthy that a variety of side products can be formed in this reaction,[6] including 6-*endo* cyclization (followed by CO_2 insertion, proposed to occur via mechanism **C**) as well as *ipso*-carboxylation (proposed to occur via pathway **D**, **Scheme 3**).

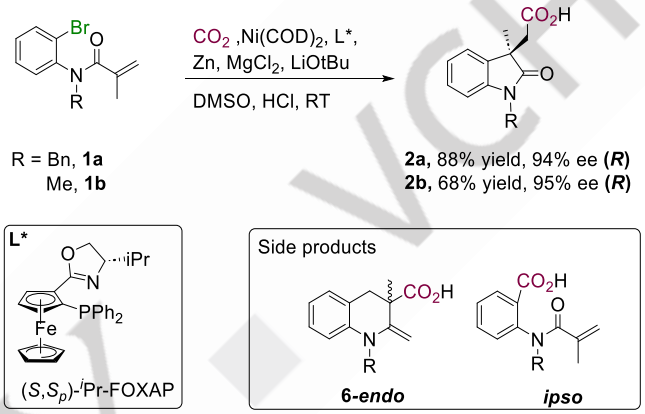

Scheme 2. Previously reported Ni-catalyzed reductive carbo-carboxylation reaction, with side products[6]

Recently, Wang and coworkers reported a computational study of the reaction described in **Scheme 2**.[15] The authors concluded that both mechanisms **A** and **B** (**Scheme 3**) may be operative, with a kinetic preference for path **B** (cyclization of the substrate *before* Ni(II) reduction). Based on the computations, the (*S*)-transition state for cyclization of substrate **1b** was reported to be preferred by 2.3 kcal/mol, translating to an *e.e.* of 96.0 % (*S*).

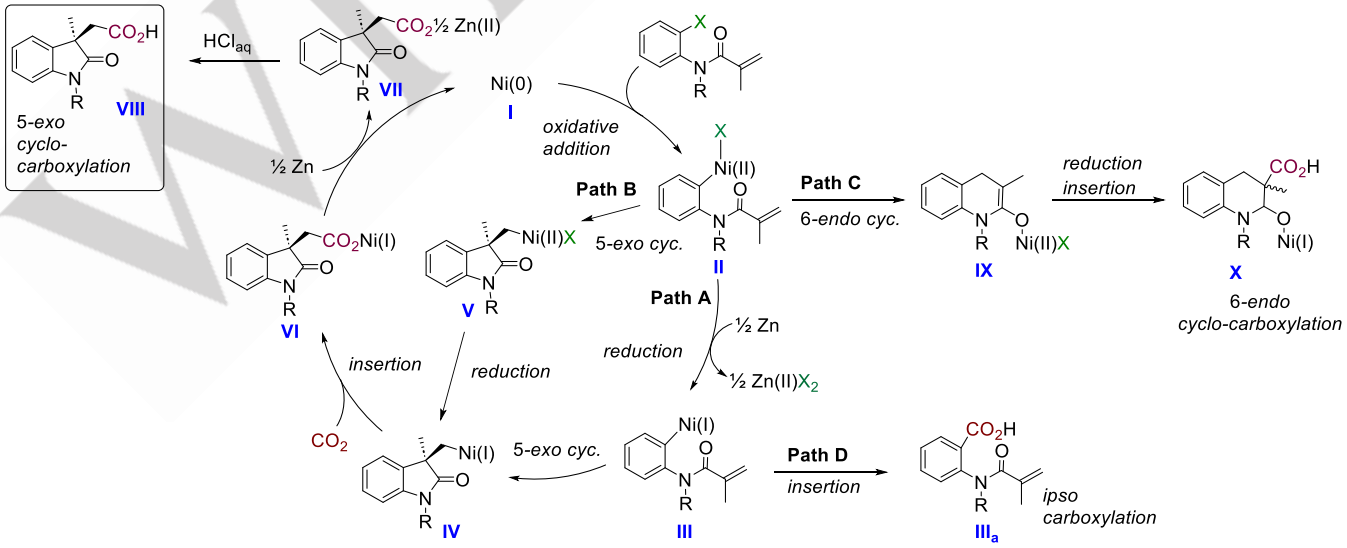

Scheme 3. Proposed pathways **A**, **B, C** and **D** for the Ni-catalyzed reductive carbo-carboxylation reaction, on basis of the previous experimental work[6]

10.1002/chem.202401631

RESEARCH ARTICLE

Intriguingly, this is the opposite stereochemical configuration than what was obtained in experiments, 95.0 % (*R*).[6] The previous computational study did not report an analysis of the preferred spin states of the involved intermediates and did not consider the effect of the additives (LiOtBu and $MgCl_2$) on the mechanism and energetics of the reaction.

Intrigued by the discrepancy between the experimentally and computationally determined enantioselectivity for the Ni-mediated reductive carbo-carboxylation reaction, we have employed state-of-the-art DFT (PBE0-D3BJ[IEFPCM]) methods to revisit the mechanism for the reaction in **Scheme 2**. We show that the preferred spin state for the Ni(II) complex is a triplet, which unambiguously favors the reaction mechanism where cyclization takes place *after* reduction (pathway **A**), reproducing the experimentally reported enantioselectivity. We further investigate the effect of Lewis acid additives and *in situ* formed salts on the mechanism and show that they may play an essential role in suppressing side reactions and promoting formation of the 5-*exo*-product.

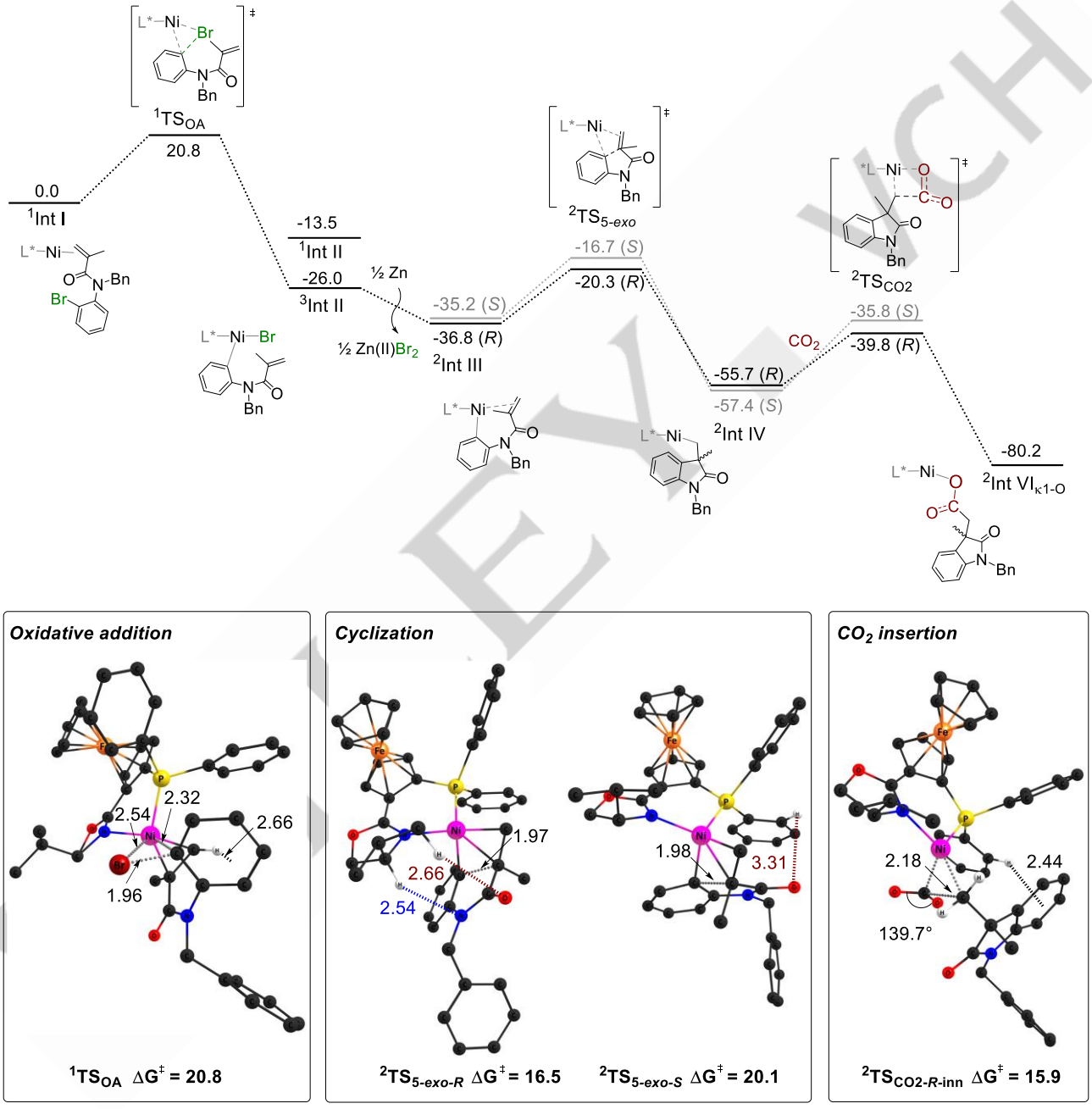

Figure 1. *Top*: The computed Gibbs free energy profile for the Ni-mediated reductive carbo-carboxylation of **1a** (Mechanism **A**) in the absence of additives. *Bottom*: Optimized geometries of ^{1}**TS**$_{OA}$, ^{2}**TS**$_{5\text{-}exo\text{-}R}$, ^{2}**TS**$_{5\text{-}exo\text{-}S}$ and ^{2}**TS**$_{CO2\text{-}R\text{-}inn}$ (298 K, kcal/mol, distances in Angstrom, hydrogen atoms omitted for clarity, PBE0-D3BJ, IEFPCM[DMSO], black: (*R*)-pathway, grey: (*S*)-pathway)

10.1002/chem.202401631

Results and Discussion

The reductive carbo-carboxylation mechanism

Initially, we employed *N*-benzyl-*N*-(2-bromophenyl)methacrylamide **1a** as a substrate with (S,S_p)-^{i}Pr-FOXAP as a chiral ligand (**Scheme 2**) to perform a comprehensive computational analysis of the mechanistic details. The computed energy profile of mechanism **A** is shown in **Figure 1**. The mechanism starts from a substrate-coordinated closed-shell singlet species Ni(0)-Sub, which is used as an energetic reference (**^{1}Int I**, **Fig**. **1**, SI, Fig. S1A). Next, a Ni(II)-(alkyl)(Br) intermediate is formed via a concerted oxidative addition step with a rate-limiting barrier of 20.8 kcal/mol (**^{1}TS$_{OA}$**, **Fig**. **1**). At ^{1}TS$_{OA}$, the substrate prefers to coordinate to nickel via the double bond (Fig. 1). If coordination occurs through the oxygen of the substrate, the barrier increases by 1.6 kcal/mol (SI, Fig. S3). Our analysis further shows that oxidative addition can occur via a triplet TS, but the barrier is 6.2 kcal/mol higher (**^{3}TS$_{OA}$**, Fig. S1B), making the singlet TS more likely. The formed alkyl intermediate, however, clearly prefers a triplet spin state (**^{3}Int II**, Fig. S2), with the closed-shell singlet state **^{1}Int II** being >12 kcal/mol higher in energy (**Fig**. **1**). The results show that a spin crossover from singlet to triplet takes place after the TS.

The subsequent Zn-mediated reduction of **^{3}Int II** provides a doublet Ni(I) species (**^{2}Int III**, (*R*), Fig. S4A), which is 10.8 kcal/mol more stable. This step was modelled assuming a solvated Zn species:[5c] ½ Zn(0)-DMSO + LNi(II)Cl -> ½ Zn(II)Cl$_2$-DMSO + LNi(I) (see SI for further details).

In the following step, the enantiodetermining 5-*exo* cyclization occurs, with a computed barrier of 16.5 kcal/mol (**^{2}TS$_{5\text{-}exo}$**, (*R*), **Fig**. **1**) to give **^{2}Int IV** ((*R*), SI, Fig. S5). At the optimized (*R*)-TS geometry, non-covalent interactions between the substrate and the ^{i}Pr-FOXAP ligand are seen (C-H/O: 2.66 Å, C-H/N: 2.54 Å, **Fig**. **1**). The (*S*)-diastereomeric **^{2}TS$_{5\text{-}exo}$** is higher in energy by 3.6 kcal/mol, which may be caused by weaker non-covalent interactions (C-H/O: 3.31 Å, **Fig**. **1**). On basis of the barrier differences, the predicted *e.e.* is 99 % (*R*), in good agreement with the experimentally observed *e.e.* of 94 % (*R*) for this substrate.[6]

Finally, CO_2 insertion into **^{2}Int IV** takes place, resulting in the formation of the κ^1-O-complex **^{2}Int VI**; a κ^2-O,O-complex is higher in energy by 0.8 kcal/mol (SI, Fig. S7). Our calculations show that CO_2 preferably inserts via an inner sphere path, with a computed barrier of 15.9 kcal/mol (**^{2}TS$_{CO2\text{-}R\text{-}inn}$**, **Fig. 1**), in line with other studies reporting inner sphere CO_2 insertion into Ni(I) complexes.[5b,8] Alternative conformations, including a two-step outer sphere CO_2 insertion, are higher in energy (Fig. S8-11). Interestingly, in the outer sphere insertion, the second step (carboxylate rotation) has a low barrier (SI, Fig. S12) in line with previous work on outer sphere C-CO_2 bond formation,[10c,16] but in contrast to CO_2 hydrogenation reactions, where the second step is rate-limiting.[17]

The alternative mechanism **B** (**Scheme 3**, **S**I, Fig. S13-15), where cyclization occurs prior to Zn-mediated reduction via **^{3}Int V** (SI, Fig. S15), gives an overall barrier of 27.4 kcal/mol (**^{3}TS$_{Iltov}$**, **S**I, Fig. S14). The significantly higher barrier compared to Mechanism **A** rules out **B** as the operative pathway.

In order to evaluate if the preference for Mechanism **A** may be substrate-dependent, we also analyzed *N*-(2-bromophenyl)-*N*-methylmethacrylamide (**1b**, **Fig. 2**). At the energetic reference **^{1}Int I**, the substrate **1b** coordinates via the double bond in an equatorial position (SI, Fig. S16). The same binding mode is found during oxidative addition via **^{1}TS$_{OA}$** (19.8 kcal/mol, SI, Fig. S17). As observed for **1a**, the formed Ni(II)-species **^{3}Int II** prefers a triplet over a closed-shell singlet state by 5.4 kcal/mol (SI, Fig. S18). From **^{3}Int II**, either reduction (mechanism **A**) or cyclization (mechanism **B**) can occur. Our results show that Zn-mediated reduction provides a low-lying Ni(I)-species (**^{2}Int III**, SI, Fig. S19), which can undergo 5-*exo* cyclization to form an (*R*)-stereogenic centre with a barrier of 15.1 kcal/mol (**^{2}TS$_{5\text{-}exo}$**, (*R*), SI, Fig. S20). The (*S*)-TS is higher in energy by 1.4 kcal/mol (SI, Fig. S20), providing a predicted *e.e.* of 83 % (*R*), in line with the experimental results (95 % (*R*)).[6] CO_2 insertion into **^{2}Int IV** ((*R*), SI, Fig. S21) has a computed barrier of 15.6 kcal/mol (SI, Fig. S22-S23). If the reaction instead follows mechanism **B**, the best cyclization TS provides the (*R*)-product (**^{1}TS$_{5\text{-}exo}$**, (*R*), SI, Fig. S24), with an overall barrier of 25.6 kcal/mol. Thus, mechanism **A** (overall barrier 19.8 kcal/mol) is preferred by 5.8 kcal/mol, also for substrate **1b**.

Comparison to previous mechanistic analysis

A previous computational study on reductive carbo-carboxylation of **1b** indicated a kinetic preference for mechanism **B**, alongside a predicted formation of the (*S*)-product.[15] This is in contrast to the results observed here, where mechanism **A** and formation of the (*R*)-product is preferred (*vide supra,* **Figure 2**). In order to better understand this discrepancy, we have reoptimized the previously reported geometries,[15] both at the previously reported computational protocol (B3LYP-D3BJ,SMD[DMSO], SI, Table S3) as well as with the main protocol employed here (PBE0-D3BJ/IEFPCM[DMSO]).

As **Figure 2** shows, our energetic reference **^{1}Int I** is 16.2 kcal/mol lower in energy than the previous reference structure, which showed substrate coordination via the phenyl ring[15] (SI, Fig. S16B). The lower reference state leads to an overall higher barrier for oxidative addition, although it can be noted that our conformation of TS$_{OA}$ is lower in energy by 2.6 kcal/mol than the previously reported geometry (**^{1}TS$_{OA\text{-}P}$**, SI, Fig. S17A). The formed Ni(II)-intermediate **^{3}Int II** prefers a triplet state in our calculations, as discussed above. Due to a lack of spin state information in the previous study,[15] we reoptimized the previous Ni(II) intermediates and cyclization TSs at the same level of theory as reported earlier (B3LYP-D3BJ/SMD[DMSO])[15] and conclude that the reported geometries most likely are singlets (for further discussion see SI, Table S3). Our optimized Ni(II)

10.1002/chem.202401631

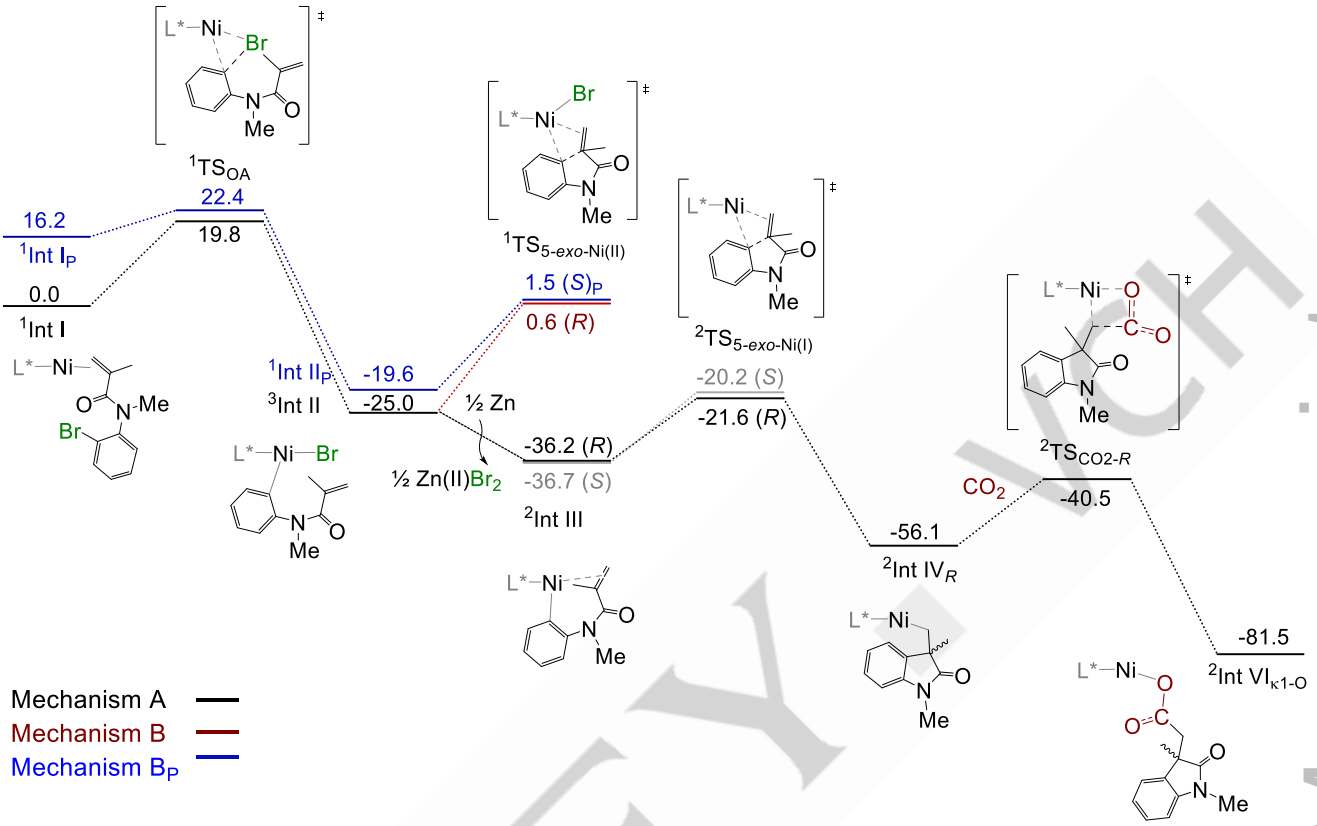

Figure 2. The computed Gibbs free energy profile for **1b**, comparing previously reported conformations (blue, Mechanism $\mathbf{B_P}$)[15] and conformations computed here (red: Mechanism **B,** black and grey: Mechanism **A**, 298 K, kcal/mol, all computed at the PBE0-D3BJ, IEFPCM[DMSO] level of theory)

cyclization TS (mechanism **B**) with (*R*)-conformation ($^1TS_{5\text{-exo-}R\text{-}Ni(II)}$) is slightly lower in energy than the previously reported best conformation, which gave the (*S*)-product ($^1TS_{5\text{-exo-}S\text{-}Ni(II)\text{-}P}$). This makes our Ni(II) cyclization TS more in line with the experimental (*R*)-selectivity, however, the overall barrier of 25.6 kcal/mol (**Fig. 2**) still indicates that mechanism **B** is less likely than mechanism **A** (barrier of 19.8 kcal/mol, **Fig. 2**). The discrepancy to previous conclusions[15] may thus be caused by a lack of spin state analysis, as well as by energetically higher-lying geometries.

Side reactions

As **Scheme 4** shows, the Ni(II)-alkyl bromide intermediate **II** and its reduced species intermediate **III** represent branching points for several putative mechanistic pathways, leading to formation of possible side products. We have explored these pathways with substrate **1a**. From intermediate **II**, a 6-*endo* cyclization can arise (mechanism **C**, SI, Fig. S25-S30), but the computed barrier is 37.5 kcal/mol (SI, Fig. S26), ruling out this possibility. Instead, we propose that the small amount of 6-*endo* cyclization observed in experiments (2 % under optimal conditions[6]) may occur *after* reduction (mechanism **E**, Scheme 4, SI, Fig. S31-32). The barriers computed here for 6-*endo* cyclization via pathway **E** (15.5 kcal/mol) and the subsequent CO_2 insertion (8.6 kcal/mol) are feasible under the reaction conditions and suggest that significant formation of the 6-*endo* product should be expected, in contrast to experiments, where the 5-*exo* product dominates. We propose that under reaction conditions, the 6-*endo* cyclization is affected by *in situ* formed salts, resulting in low amounts of 6-*endo* product (2 %)[6], as explored further below (*vide infra*). We also note that the formed 6-*endo* cyclization product may undergo a β-hydride elimination, but the computed barrier of 20.1 kcal/mol (SI, Fig. S33-35) make it less likely than CO_2 insertion.

Finally, *ipso* carboxylation can take place from intermediate **III**, with a computed inner sphere insertion barrier of 21.9 kcal/mol (mechanism **D**, SI, Fig. S36-39), which is 5.4 kcal/mol higher than formation of the 5-*exo* product (cyclization barrier of 16.5 kcal/mol, **Fig. 1**). The results are in line with the small amounts of *ipso*-product observed in experiments (3 % under optimal conditions[6]). Outer sphere CO_2 insertion is higher by 4.9 kcal/mol (SI, Fig. S38), in line with previous computational

10.1002/chem.202401631

studies where C_{sp2} systems favor inner sphere CO_2 insertion.[9a,9c]

Overall, our mechanistic analysis of side reactions is in line with experimental results, but indicates that after formation of intermediate **III**, undesired 6-*endo* cyclization (barrier 15.5 kcal/mol) appears favored by 1.0 kcal/mol relative to 5-*exo* cyclization (barrier 16.5 kcal/mol, **Fig**. **1**), which is not in agreement with experiments, where mostly the later product was formed.[6] In order to understand this discrepancy, we turned to exploring the effect of additives on the reaction mechanism.

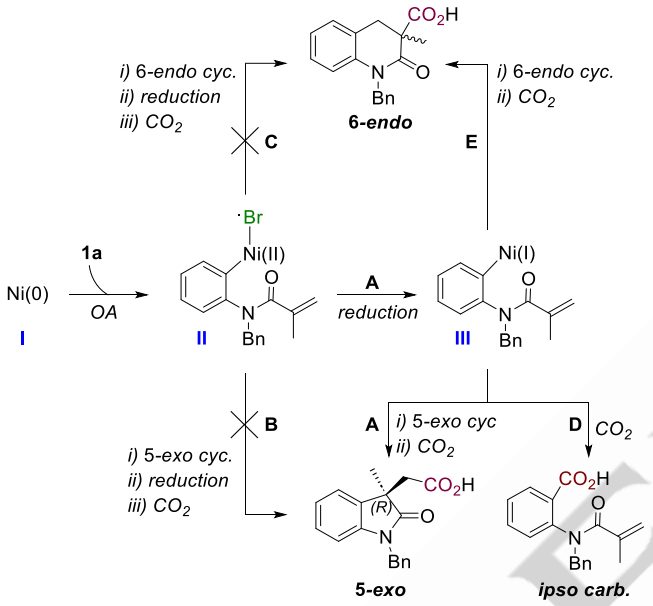

Scheme 4. Possible pathways for formation of experimentally observed products.[6] Pathways C and B are excluded here based on computational results, instead the dominant pathways are proposed to be A (5-*exo*), D (ipso) and E (6-*endo*).

Effect of additives

Experimentally, the asymmetric Ni-mediated carbo-carboxylation of methacrylamides with CO_2 was performed in the presence of Zn, $MgCl_2$ and LiOtBu.[6] If either $MgCl_2$ or LiOtBu were removed, lower yields were obtained.[6] Lack of Zn lead to a variety of side products, with increased formation of the 6-*endo* compound.[6]

We note that the additives have the potential to be transformed *in situ* to different salts: Zn is acting as reducing agent, resulting in formation of ZnX_2 (X = Br, Cl). In addition, $MgCl_2$ may react with LiOtBu, forming new species such as MgOtBuCl and LiCl. $MgCl_2$, which has low solubility in aprotic polar organic solvents[18] may also form clusters such as the dimer Mg_2Cl_4 (SI, Fig. S63-S70) as seen in reported crystal structures.[19] Thus, we investigated the role that different added and *in situ* formed salts ($ZnBr_2$, $ZnCl_2$, $MgCl_2$, Mg_2Cl_4, MgOtBuCl, LiOtBu) may have during the catalytic cycle. Initially, we evaluated which of these salts bind stronger to **Int I**, assuming that Lewis acids have a strong potential to interact with the carbonyl group of the methacrylamide substrate. The computed binding energies show that Mg salts (MgOtBuCl and $MgCl_2$) bind stronger (in the range of 9.2 to 9.6 kcal/mol) than Zn or Li salts (SI, Table S1). Thus, as a first step towards understanding the role of LAs on the reaction mechanism, we modelled the full mechanism **A** for substrate **1a** in presence of $MgCl_2$ (SI, Fig. S40-49), with the energy profile shown in **Figure 3**. Additionally, critical steps were modelled with MgOtBuCl, LiOtBu, Mg_2Cl_4, $ZnBr_2$ and $ZnCl_2$ (SI, Fig. S40-S83). We note that the overall mechanistic steps are preserved in presence of Lewis acids, however, a detailed analysis of each step (*vide infra*) shows that the different salts may have different effects on the computed barriers, and hence on the product selectivity.

Effect of additives on oxidative addition

Lack of LiOtBu or $MgCl_2$ reduces experimental reaction yields by 25 to 45 %;[6] this may be due to an effect on the rate-limiting step, which we identified as oxidative addition ($^1TS_{OA}$, **Fig. 1**). However, the computed OA barriers in the presence of $MgCl_2$, LiOtBu, or *in situ* formed species MgOtBuCl or $ZnBr_2$ are all in the range 20.9 - 21.1 kcal/mol (**Fig. 3**, SI, Fig. S54, S56, S72), essential identical to the value in absence of additives (20.8 kcal/mol, **Fig**. **1**). $MgCl_2$ neither plays a role in stabilizing the liberated bromide during formation of **^{3}Int II**, as a computed TS conformation where Mg(II) interacts with bromide displays an energetically inaccessible barrier of 45.0 kcal/mol (SI, Fig. S50). Only for the dimer Mg_2Cl_4, we computed a barrier reduction for the OA-step of 2.2 kcal/mol (SI, Fig. S64), indicating that the speciation of the LA may affect the overall barrier.

Effect of additives on the cyclization step

Initially, we investigated how the presence of distinct additives affects the competition between 5-*exo* and 6-*endo* cyclization. Experimental stoichiometric tests in the absence of CO_2 and in the presence of $MgCl_2$ and LiOtBu have shown that under very low Zn loadings or in the absence of Zn, 6-*endo* cyclization dominates, whereas higher amounts of Zn favor the 5-*exo* species.[6] This indicates that the amount of Zn plays an important role in the product selectivity.[6] Based on our computational results, both the 5-*exo* and the 6-*endo* product can be formed from the reduced Ni(I)-aryl species **Int III** (**Scheme 4**), thus it is not the reduction step itself that controls the product selectivity. Instead, we speculate that the $ZnBr_2$ species, which is likely generated *in situ*, may affect cyclization. Indeed, in the presence of $ZnBr_2$, the computed barrier for 5-*exo* cyclization is 2.0 kcal/mol lower than the 6-*endo* cyclization (**Fig. 4A**). At the 5-*exo*-TS in presence of $ZnBr_2$ (**Fig. 4A**), we observe a three-center two-electron interaction (Zn···H-C, 2.07 Å) as well as a C-H/O (2.63 Å) and a C-H/N (2.58 Å) interaction. Interestingly, Zn(II) interacts with the terminal C-atom of the substrate double bond (2.11 Å) and an oxygen of the CO group (2.17 Å). At the 6-*endo*-TS in presence of $ZnBr_2$ (**Fig. 4C**), Zn(II) interacts with an oxygen of the CO (1.93 Å) but no significant C-H/O and C-H/N interactions or Zn(II)-binding to the terminal C atom are seen. In order to obtain further insights into the non-

10.1002/chem.202401631

RESEARCH ARTICLE

covalent interactions at the optimized TS structures, we performed an NCI analysis[20] of the *endo* and *exo* cyclization TSs (see SI, Fig. S84). At the pro-(*R*) exo cyclization TS, C-H/N and C-H/O interactions are highlighted (SI, Fig. S84A). The NCI analysis further indicates that the Zn-C interaction, present at both pro-(*R*) and pro-(*S*) *exo*-TSs, is strongly attractive (SI, Fig. S84A). This interaction is absent at the *endo*-TS (SI, Fig. S84B).

Based on our combined results, we propose that during 5-*exo* cyclization, Zn(II) provides better stabilization of the emerging negative charge on the terminal C atom compared to the other salts, as it makes stronger interactions than Mg(II) or Li(I) (Zn-C: 2.11 Å **Fig. 4A**, Mg-C: 2.32 Å **Fig. 3**, Li-C: 2.87 Å, SI, Fig. S58). This is supported by the fact that the 5-*exo* cyclization TS in presence of $ZnBr_2$ is 2.8 kcal/mol lower in energy than the equivalent TS in presence of $MgCl_2$ (see SI, Scheme S1) and 7.7 kcal/mol lower than the TS in the absence of LAs (**Fig. 1**). In order to test if other Zn salts may have a similar effect, we also

.

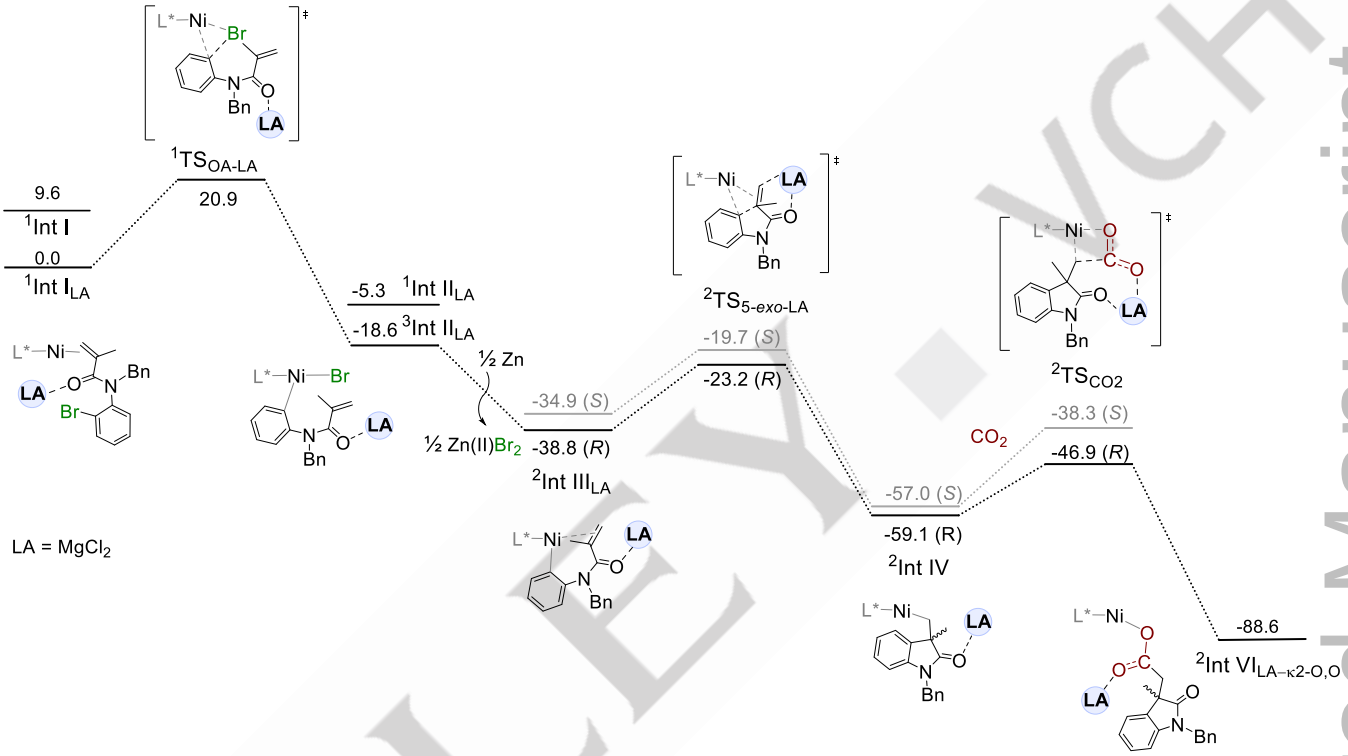

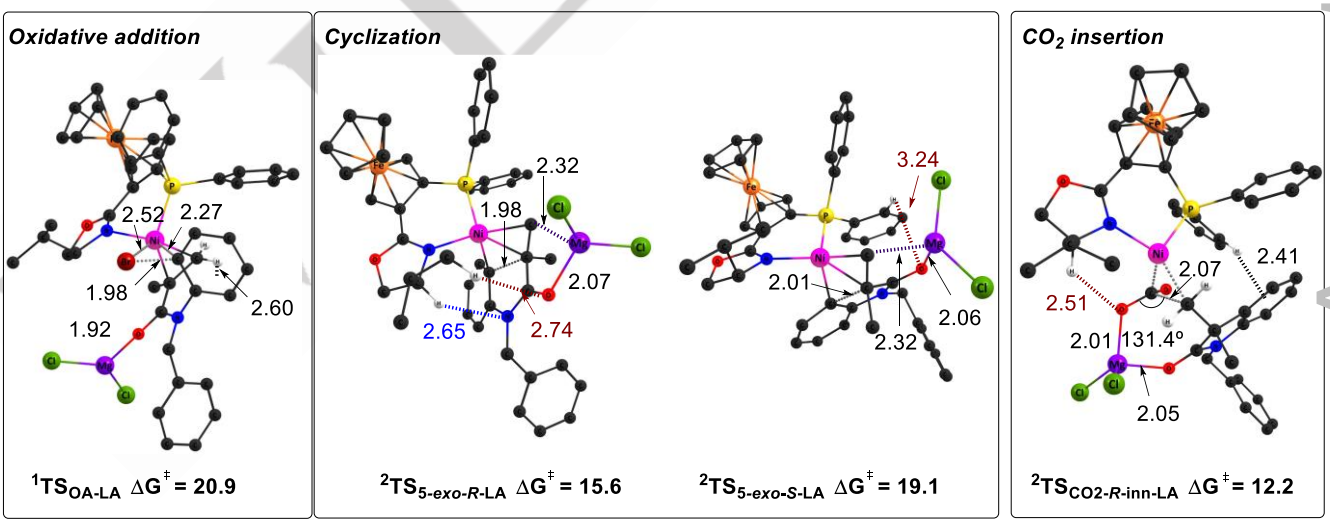

Figure 3. *Top:* The Gibbs free energy profile (Mechanism **A**) for Ni-mediated reductive carbo-carboxylation of **1a** in the presence of $MgCl_2$. The energetic reference ^{1}**Int**$_{LA}$ is 9.6 kcal/mol lower in energy than ^{1}**Int** computed in the absence of $MgCl_2$ (Figure 1). *Bottom:* Optimized geometries of ^{1}**TS**$_{OA\text{-}LA}$, ^{2}**TS**$_{5\text{-}exo\text{-}R\text{-}LA}$, ^{2}**TS**$_{5\text{-}exo\text{-}S\text{-}LA}$ and ^{2}**TS**$_{CO2\text{-}R\text{-}inn\text{-}LA}$ (298K, kcal/mol, distances in Angstrom, hydrogen atoms omitted for clarity, PBE0-D3BJ, IEFPCM[DMSO]).

10.1002/chem.202401631

computed the TSs in presence of $ZnCl_2$ and the same trend is observed, where 5-*exo* cyclization is preferred by 2.2 kcal/mol relative to the 6-*endo* cyclization (SI, Fig. S83), indicating that different Zn salts can affect the product selectivity.

We note that calculations with other additives ($MgCl_2$, LiOtBu, Mg_2Cl_4, **Fig.3**, SI, Fig. S51, S58, S60, S65-S66) show that only $ZnBr_2$ and $ZnCl_2$ result in preferred 5-*exo* cyclization. Further, the enantioselectivity of 5-*exo* cyclization is preserved in presence of $ZnBr_2$, with the (*R*)-TS displaying a 3.2 kcal/mol lower barrier than the (*S*)-TS (**Fig. 4,** SI, Fig. S82), compared to 3.6 kcal/mol in absence of LAs (**Fig. 1**).[21] This is in agreement with experiments, where it has been shown that the *e.e.* is essentially unaffected by the presence of additives.[6]

Effect of additives on CO_2 insertion

For LA-mediated CO_2 activation, we have previously shown that Zn(II) salts do not have a beneficial effect.[10a] Indeed, the computed barrier for CO_2 insertion in the presence of $ZnBr_2$ is 24.0 kcal/mol (Fig. S77-S80), which is higher than in absence of additives (15.9 kcal/mol, **Fig. 1**). On the other hand, Li(I) and Mg(II) cations are predicted to provide good CO_2 activation.[5c,17]

Indeed, in presence of $MgCl_2$, Mg_2Cl_4 or LiOtBu, the barriers for C-CO_2 bond formation are reduced from 15.9 kcal/mol to 12.2 kcal/mol (**Fig. 3**), 14.7 kcal/mol (SI, Fig. S62) and 15.2 kcal/mol (SI, Fig. S70) for these three salts, respectively. $MgCl_2$ shows the strongest effect, with the optimized TSs displaying an inner sphere mechanism, where Mg(II) interacts with one oxygen of CO_2 and the oxygen of the carbonyl group of the substrate (outer sphere TSs are higher in energy, SI, Fig. S45-47). We also explored if CO_2 insertion could occur at Mg(II), assuming formation of a Grignard-type complex (SI, Fig. S48), but the computed barrier of 22.8 kcal/mol is higher than Ni-mediated CO_2 insertion (12.2 kcal/mol, **Fig. 3**). Finally, in presence of $MgCl_2$, the Ni(I) product complex (**Fig. 3**) shows preferred κ^2-O,O-coordination of the carboxylate group, in contrast to the k^1-O complex preferred in absence of additives (SI, Fig. S23, S49).

In summary, the detailed mechanistic analysis of additives and *in situ* formed salts support different roles for these: The rate-limiting OA step is essentially unaffected by the presence of salts, except for Mg_2Cl_4, which lowers the OA barrier slightly, although we cannot know if such a species indeed will be formed *in situ*. The experimental formation of $ZnBr_2$ on the other hand is strongly expected, and our results show that it promotes 5-*exo* cyclization over 6-*endo* cyclization, which may explain the 6-*endo* preference observed experimentally under low Zn loadings.[6] The $MgCl_2$ and LiOtBu additives both strongly promote CO_2 insertion, in line with other results showing that Li(I) and Mg(II) are superior in activating CO_2.[5c,17]

Conclusion

DFT calculations were conducted to elucidate the mechanistic details of the asymmetric Ni-catalyzed reductive carbo-carboxylation of methacrylamides with CO_2. Our computations show that the main mechanism **A** follows these steps: i) oxidative addition of the substrate to Ni(0) to form a triplet Ni(II)-(aryl)(Br) species, ii) Zn-mediated reduction to generate a doublet Ni(I)-aryl complex, iii) cyclization to form a Ni(I)-5-*exo*-intermediate, and iv)

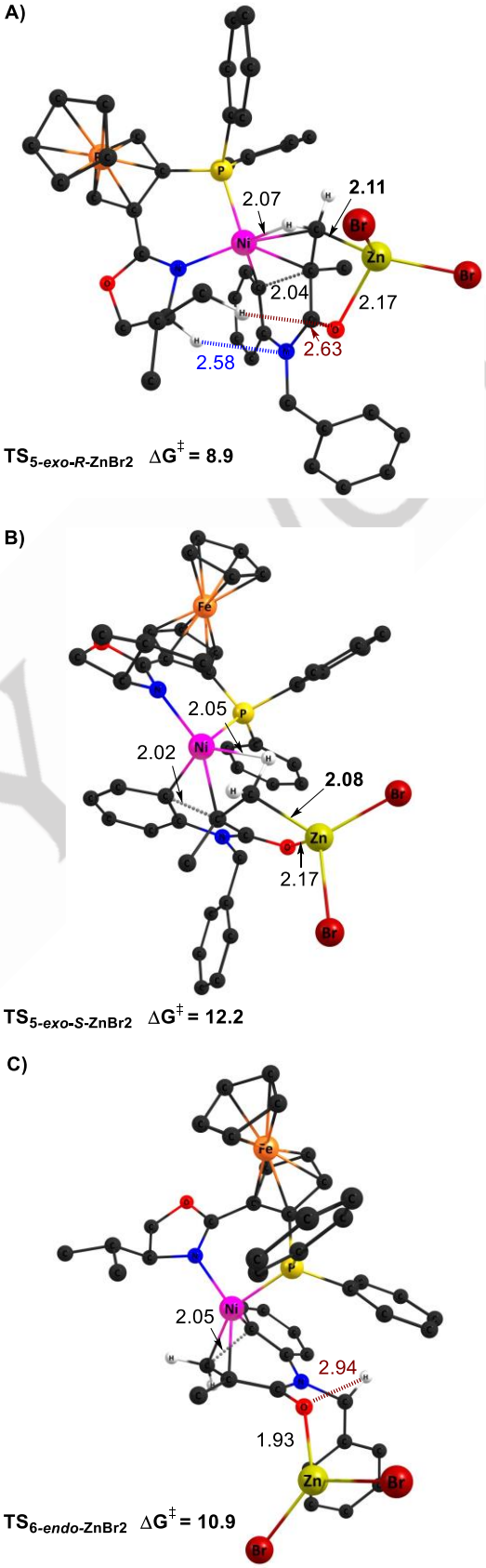

Figure 4. Optimized geometries for (A) (*R*)-5-*exo*, (B) (*S*)-5-*exo* and C) 6-*endo* cyclization in presence of $ZnBr_2$ (kcal/mol, distances in Angstrom, hydrogen atoms are omitted for clarity PBE0-D3BJ, IEFPCM[DMSO]).

inner sphere CO_2 insertion to give the Ni(I)-carboxylate. For both studied substrates, the rate-limiting step is the oxidative addition, whereas the selectivity-determining step is 5-*exo* cyclization. The enantioselectivity is controlled via C-H/O and C-H/N interactions, with our computed ***e.e.'s*** (**1a** 99 % (*R*); **1b** 83 % (*R*)) being in line with the experimentally reported ***e.e.'s*** (94-95 % (*R*))[6], resolving the previously reported discrepancy between computed[15] and experimental[6] enantioselectivities.

Our detailed analysis of additives indicates that Zn(II) salts favor formation of the 6-*endo* product, in agreement with experimental results, showing that lack of Zn results in increased 6-*endo* cyclization.[6] In line with our earlier results, Zn(II) has no beneficial effect on the CO_2 insertion barrier, however, this step is significantly accelerated in the presence of Li(I) or Mg(II)-salts. Overall, our computational analysis provides a comprehensive picture of how additives can affect the mechanistic outcome by influencing different reaction steps. The role of LAs in activation of CO_2 is also supported by our work.

Computational details

The Gaussian 16, Rev. B.01 software package was used to carry out calculations.[22] Geometries of all intermediates and TSs were fully optimized, without any truncations, by employing the DFT functional PBE0[23], including Grimme's empirical dispersion correction D3BJ[24] and the IEFPCM solvent model (DMSO)[25]. The split-valence double-zeta Ahlrichs basis set def2-SVP (BS1)[26] was employed for all atoms, whereas for single point electronic energy calculations, def2-TZVP (BS2) was used. We carefully explored the conformational space through optimization of multiple configurations. The energetically preferred geometries are reported in the main text, whereas relevant higher lying geometries are given in the SI.

For comparison, we also tested additional computational protocols, including B3LYP-D3[24,27] (see SI, [24,27]Tables S2-S8) and B3LYP-D3BJ/SMD[DMSO] (SI, Table S3).

[26]

Reported Gibbs free energies correspond to:

$$\Delta G_{1atm,\ 298K,BS2} = \Delta G_{1atm,\ 298K,BS1} - \Delta E_{1atm,BS1} + \Delta E_{1atm,BS2}$$

The theoretical enantiomeric excess was computed using the following formula:[28]

$$ee_{theo} = \frac{1-e^{(-\Delta\Delta G\neq/RT)}}{1+e^{(-\Delta\Delta G\neq/RT)}}$$

The non-covalent interactions were analyzed with the NCIPLOT 4.0 program.[20]

Supporting Information

- Optimized coordinates, which can be visualized with the Mercury program from the Cambridge Crystallographic Data Centre (XYZ file)
- Additional computational results, as described in the main text (PDF)

Acknowledgment

We gratefully acknowledge support from the Research Council of Norway (No. 300769), Sigma2 (No. nn9330k, nn4654k) NordForsk (No. 85378) and the European Union's Horizon 2020 research and innovation programme under the Marie Skłodowska-Curie grant agreement (No. 859910). We thank Sahil Gahlawat who assisted in the NCI analysis.

Conflict of Interest

The authors declare no conflict of interest.

Keywords: Carboxylation • DFT • Lewis acids • CO_2

References

[1] a) A. S. Shukla P, Ashok S., *Biorg. Org. Chem.* **2017**, *1*, 70-79; b) J. Iglesias, I. Martínez-Salazar, P. Maireles-Torres, D. Martin Alonso, R. Mariscal, M. López Granados, *Chem. Soc. Rev.* **2020**, *49*, 5704-5771; c) K. Bredael, S. Geurs, D. Clarisse, K. De Bosscher, M. D'hooghe, *J. Chem.* **2022**, 2164558; d) M. Y. Low, G. Koutsidis, J. K. Parker, J. S. Elmore, A. T. Dodson, D. S. Mottram, *J. Agric. Food Chem.* **2006**, *54*, 5976-5983.

[2] a) C. Ballatore, D. M. Huryn, A. B. Smith III, *Chem. Med. Chem.* **2013**, *8*, 385-395; b) S. Erol Gunal, S. Teke Tuncel, I. Dogan, *Tetrahedron* **2020**, *76*, 131141.

[3] a) C. M. Williams, J. B. Johnson, T. Rovis, *J. Am. Chem. Soc.* **2008**, *130*, 14936-14937; b) A. Correa, R. Martín, *J. Am. Chem. Soc.* **2009**, *131*, 15974-15975; c) A. Correa, R. Martín, *Angew. Chem. Int. Ed.* **2009**, *48*, 6201-6204; d) T. León, A. Correa, R. Martin, *J. Am. Chem. Soc.* **2013**, *135*, 1221-1224; e) Y. Liu, J. Cornella, R. Martin, *J. Am. Chem. Soc.* **2014**, *136*, 11212-11215; f) X. Wang, Y. Liu, R. Martin, *J. Am. Chem. Soc.* **2015**, *137*, 6476-6479; g) M. Börjesson, T. Moragas, R. Martin, *J. Am. Chem. Soc.* **2016**, *138*, 7504-7507; h) A. Tortajada, F. Juliá-Hernández, M. Börjesson, T. Moragas, R. Martin, *Angew. Chem. Int. Ed.* **2018**, *57*, 15948-15982; i) H. Tran-Vu, O. Daugulis, *ACS Catal.* **2013**, *3*, 2417-2420; j) Y. Tsuji, T. Fujihara, *Chem. Commun.* **2012**, *48*, 9956-9964; k) T. Fujihara, K. Nogi, T. Xu, J. Terao, Y. Tsuji, *J. Am. Chem. Soc.* **2012**, *134*, 9106-9109; l) C. Maeda, Y. Miyazaki, T. Ema, *Catal. Sci. Technol.* **2014**, *4*, 1482-1497; m) M. Börjesson, T. Moragas, D. Gallego, R. Martin, *ACS Catal.* **2016**, *6*, 6739-6749; n) R. Martín, A. W. Kleij *Chem. Sus. Chem.* **2011**, *4*, 1259-1263; o) G. Bertuzzi, A. Cerveri, L. Lombardi, M. Bandini, *Chin. J. Chem.* **2021**, *39*, 3116-3126; p) A. Cerveri, R. Giovanelli, D. Sella, R. Pedrazzani, M. Monari, O. Nieto Faza, C. S. López, M. Bandini, *Chem. Eur. J.* **2021**, *27*, 7657-7662; q) C.-K. Ran, X.-W. Chen, Y.-Y. Gui, J. Liu, L. Song, K. Ren, D.-G. Yu, *Sci. China Chem.* **2020**, *63*, 1336-1351; r) J.-H. Ye, T. Ju, H. Huang, L.-L. Liao, D.-G. Yu, *Acc. Chem. Res.* **2021**, *54*, 2518-2531; s) X.-W. Chen, L. Zhu, Y.-Y. Gui, K. Jing, Y.-X. Jiang, Z.-Y. Bo, Y. Lan, J. Li, D.-G. Yu, *J. Am. Chem. Soc.* **2019**, *141*, 18825-18835.

[4] T. Moragas, R. Martin, *Synthesis* **2016**, *48*, 2816-2822.

[5] a) D. J. Charboneau, G. W. Brudvig, N. Hazari, H. M. C. Lant, A. K. Saydjari, *ACS Catal.* **2019**, *9*, 3228-3241; b) F. B. Sayyed, Y. Tsuji, S. Sakaki, *Chem. Commun.* **2013**, *49*, 10715-10717; c) F. B. Sayyed, S. Sakaki, *Chem. Commun.* **2014**, *50*, 13026-13029; d) P. Vadivelu, K. Ganesan, *Inorg. Chem.* **2022**, *61*, 19463-19474.

[6] X.-W. Chen, J.-P. Yue, K. Wang, Y.-Y. Gui, Y.-N. Niu, J. Liu, C.-K. Ran, W. Kong, W.-J. Zhou, D.-G. Yu, *Angew. Chem. Int. Ed.* **2021**, *60*, 14068-14075.

[7] K. Nogi, T. Fujihara, J. Terao, Y. Tsuji, *J. Org. Chem.* **2015**, *80*, 11618-11623.

[8] R. J. Somerville, C. Odena, M. F. Obst, N. Hazari, K. H. Hopmann, R. Martin, *J. Am. Chem. Soc.* **2020**, *142*, 10936-10941.

[9] a) D. García-López, Lj. Pavlovic, K. H. Hopmann, *Organometallics* **2020**, *39*, 1339-1347; b) M. F. Obst, A.

Gevorgyan, A. Bayer, K. H. Hopmann, *Organometallics* **2020**, *39*, 1545-1552; c) M. Obst, Lj. Pavlovic, K. H. Hopmann, *J. Organomet. Chem.* **2018**, *864*, 115-127.

[10] a) Lj. Pavlovic, J. Vaitla, A. Bayer, K. H. Hopmann, *Organometallics* **2018**, *37*, 941-948; b) Lj. Pavlovic, M. Pettersen, A. Gevorgyan, J. Vaitla, A. Bayer, K. H. Hopmann, *Eur. J. Org. Chem.* **2021**, *2021*, 663-670; c) A. P. Deziel, M. R. Espinosa, Lj. Pavlovic, D. J. Charboneau, N. Hazari, K. H. Hopmann, B. Q. Mercado, *Chem. Sci.* **2022**, *13*, 2391-2404.

[11] S. Zhang, W.-Q. Chen, A. Yu, L.-N. He, *Chem. Cat. Chem.* **2015**, *7*, 3972-3977.

[12] Q. Pan, Y. Ping, Y. Wang, Y. Guo, W. Kong, *J. Am. Chem. Soc.* **2021**, *143*, 10282-10291.

[13] M. Yang, N. Liu, Z. Zhang, Y.-B. She, Y.-F. Yang, *ACS Catal.* **2022**, *12*, 4131-4140.

[14] Y. M. Khetmalis, M. Shivani, S. Murugesan, K. V. G. Chandra Sekhar, *Biomed. Pharmacother.* **2021**, *141*, 111842.

[15] H.-Q. Yang, Y.-N. Hou, J.-Y. Chen, S.-Q. Guo, H.-X. Yang, X. Wang, *Tetrahedron Lett.* **2023**, *129*, 154741.

[16] T. J. Schmeier, N. Hazari, C. D. Incarvito, J. A. Raskatov, *Chem. Comm.* **2011**, *47*, 1824-1826.

[17] Lj. Pavlovic, K. H. Hopmann, *Organometallics* **2023**, *42*, 3025-3035.

[18] a) L. Zeng, Z. Li, X. Wang, *J. Chem. Eng. Data* **2016**, *61*, 797-805; b) C. Liao, N. Sa, B. Key, A. K. Burrell, L. Cheng, L. A. Curtiss, J. T. Vaughey, J.-J. Woo, L. Hu, B. Pan, Z. Zhang, *J. Mater. Chem. A* **2015**, *3*, 6082-6087.

[19] a) M. Metzler, M. Bolte, M. Wagner, H.-W. Lerner, *Acta Crystallogr. E: Crystallogr. Commun.* **2023**, *79*, 341-344; b) V. H. Nissinen, I. O. Koshevoy, T. T. Pakkanen, *Dalton Trans.* **2017**, *46*, 4452-4460; c) M. Salama, I. Shterenberg, L. J.W. Shimon, K. Keinan-Adamsky, M. Afri, Y. Gofer, D. Aurbach, *J. Phys. Chem. C* **2017**, *121*, 24909-24918.

[20] R. A. Boto, F. Peccati, R. Laplaza, C. Quan, A. Carbone, J. P. Piquemal, Y. Maday, A. J. Contreras-Garcı, *J. Chem. Theory Comput.* **2020**, *16*, 4150-4158.

[21] A similar result is obtained in presence of $MgCl_2$ (Fig. 3).

[22] M. J. Frisch, G. W. Trucks, H. B. Schlegel, G. E. Scuseria, M. A. Robb, J. R. Cheeseman, G. Scalmani, V. Barone, G. A. Petersson, H. Nakatsuji, X. Li, M. Caricato, A. V. Marenich, J. Bloino, B. G. Janesko, R. Gomperts, B. Mennucci, H. P. Hratchian, J. V. Ortiz, A. F. Izmaylov, J. L. Sonnenberg, D. Williams-Young, F. Ding, F. Lipparini, F. Egidi, J. Goings, B. Peng, A. Petrone, T. Henderson, D. Ranasinghe, V. G. Zakrzewski, J. Gao, N. Rega, G. Zheng, W. Liang, M. Hada, M. Ehara, K. Toyota, R. Fukuda, J. Hasegawa, M. Ishida, T. Nakajima, Y. Honda, O. Kitao, H. Nakai, T. Vreven, K. Throssell, J. A. Montgomery, Jr., J. E. Peralta, F. Ogliaro, M. J. Bearpark, J. J. Heyd, E. N. Brothers, K. N. Kudin, V. N. Staroverov, T. A. Keith, R. Kobayashi, J. Normand, K. Raghavachari, A. P. Rendell, J. C. Burant, S. S. Iyengar, J. Tomasi, M. Cossi, J. M. Millam, M. Klene, C. Adamo, R. Cammi, J. W. Ochterski, R. L. Martin, K. Morokuma, O. Farkas, J. B. Foresman, and D. J. Fox, *Gaussian 16 Rev. B.01*, Wallingford, CT, **2016**.

[23] a) J. P. Perdew, M. Ernzerhof, K. Burke, *J. Chem. Phys.* **1996**, *105*, 9982-9985; b) C. Adamo, V. Barone, *J. Chem. Phys* **1999**, *110*, 6158-6170.

[24] S. Grimme, S. Ehrlich, L. Goerigk, *J. Comput. Chem.* **2011**, *32*, 1456-1465.

[25] J. Tomasi, B. Mennucci, R. Cammi, *Chem. Rev.* **2005**, *105*, 2999-3094.

[26] F. Weigend, R. Ahlrichs, *Phys. Chem. Chem. Phys.* **2005**, *7*, 3297-3305.

[27] A. D. Becke, *Phys. Rev. A* **1988**, *38*, 3098-3100.

[28] a) Q. Peng, F. Duarte, R. S. Paton, *Chem. Soc. Rev.* **2016**, *45*, 6093-6107; b) K. H. Hopmann, *Int. J. Quantum Chem.* **2015**, *115*, 1232-1249.

Entry for the Table of Contents

Ni-catalyzed reductive carbo-carboxylation:
Lewis acids affect the product selectivity

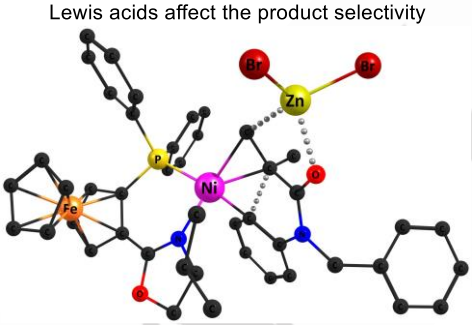

DFT methods were used to revisit the mechanism of the Ni-catalyzed reductive carbo-carboxylation of alkenes with CO_2. Our results indicate that zinc salts can alter the product selectivity, whereas Mg(II) and Li(I) salts activate CO_2 during C-CO_2 bond formation.

Institute and/or researcher Twitter usernames: UiT Norges arktiske universitet (@UiTNorgesarktis)